

Edge-Guided Resolution Enhancement in Projectors via Optical Pixel Sharing

Behzad Sajadi *

Department of Computer Science
University of California, Irvine

M. Gopi †

Department of Computer Science
University of California, Irvine

Aditi Majumder‡

Department of Computer Science
University of California, Irvine

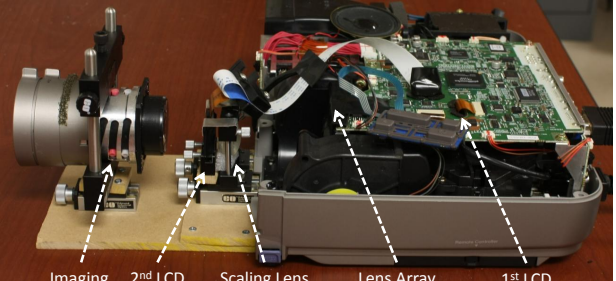
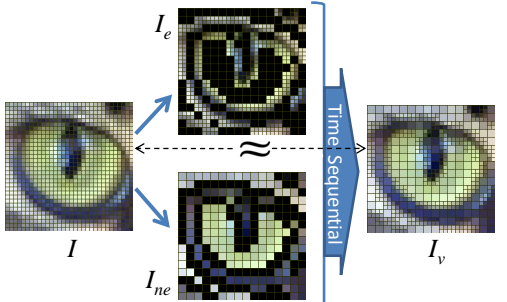


Figure 1: Left: This illustrates the basic concept of decomposing a target high resolution image, I , to a high resolution edge image, I_e and a complementary low resolution non-edge image, I_{ne} . I_e and I_{ne} are then displayed in a time sequential manner to create an image with spatially varying resolution where edges are displayed at a higher pixel density than the rest of the image. We call this the edge-enhanced image, I_v . I_v is perceptually close to I . Middle: The image from the enhanced-resolution projector compared with a target high-resolution image and a low resolution image. Note that the edge-enhanced image is perceptually almost indistinguishable from the target high-resolution image. Right: A side view of our prototype enhanced-resolution projector that achieves 1024 × 768 edge-enhanced images by cascading two light modulator panels of 512 × 384 resolution (animated illustrations in the video). The numbers in the image are in millimeters.

Abstract

Digital projection technology has improved significantly in recent years. But, the relationship of cost with respect to available resolution in projectors is still super-linear. In this paper, we present a method that uses projector light modulator panels (e.g. LCD or DMD panels) of resolution $n \times n$ to create a perceptually close match to a target higher resolution $cn \times cn$ image, where c is a small integer greater than 1. This is achieved by enhancing the resolution using smaller pixels at specific regions of interest like edges.

A target high resolution image ($cn \times cn$) is first decomposed into (a) a high resolution ($cn \times cn$) but sparse *edge image*, and (b) a complementary lower resolution ($n \times n$) *non-edge image*. These images are then projected in a time sequential manner at a high frame rate to create an *edge-enhanced image* – an image where the pixel density is not uniform but changes spatially. In 3D ready projectors with readily available refresh rate of 120Hz, such a temporal multiplexing is imperceptible to the user and the edge-enhanced image is perceptually almost identical to the target high resolution image.

To create the higher resolution edge image, we introduce the concept of *optical pixel sharing*. This reduces the projected pixel size by a factor of $\frac{1}{c^2}$ while increasing the pixel density by c^2 at the edges enabling true higher resolution edges. Due to the sparsity of the edge pixels in an image we are able to choose a sufficiently

large subset of these to be displayed at the higher resolution using perceptual parameters. We present a statistical analysis quantifying the expected number of pixels that will be reproduced at the higher resolution and verify it for different types of images.

Keywords: computational photography, computational displays, projection devices, high-resolution displays

1 Introduction

The recent years have seen a tremendous development in projector image quality, in terms of brightness, contrast and resolution. But, the relationship of cost with respect to available resolution in projectors is still super-linear. While a typical 2 Megapixel projector (e.g. Epson Home Cinema 8500 UB HD projector) costs around \$2500 today, a 4 Megapixel projector (e.g. Projection Design Cineo 35) costs around \$35,000. Thus, cost increases by more than a factor of 10 while resolution just doubles.

In this paper, we show that we can use two lower resolution light modulator panels (e.g. LCD or DMD panels) of resolution $n \times n$ (assuming square panels without loss of generality) to design a projector that can display images that provide a close perceptual match to a higher resolution display of resolution $cn \times cn$ where c is a small integer greater than 1. Our design uses a novel optical unit that can provide spatially variable pixel density across an image by realizing higher pixel density at specific areas of the image (Section 3). Since edges are known to be perceptually important [Valois and Valois 1990], we enhance the resolution of the image at the *edges* to create an *edge-enhanced image* (Figure 1).

We observe that a display with higher resolution targeted only at pixels where the high frequency content is concentrated is sufficient to create an image that is perceptually almost identical to one produced by a true higher resolution display (Figure 2). Typically, the higher frequency content in an image is given by a small set of pixels at the edges. We decompose our target high resolution ($cn \times cn$) image into two images. We identify a set of edge pixels to create a higher resolution ($cn \times cn$) *edge image* (Section 3.1). The rest of the image, complementary to the edge image, is called the *non-edge* image and is reproduced at the lower resolution ($n \times n$). These two

*e-mail: bsajadi@uci.edu

†e-mail:gopi@ics.uci.edu

‡e-mail: majumder@ics.uci.edu



Figure 2: Columns 1 and 2 show the results on a *BUILDING* image, 3 and 4 show the results on a *PEOPLE* image ($c = 2$). Top row: target high resolution image (I) and the chosen edge pixels. Bottom row: low resolution image I_l ; and its CIELAB ΔE difference from I . Middle row: edge-enhanced image, I_v , i.e. the output of our system, created by superimposing I_e and I_{ne} ; and the CIELAB ΔE of I_v from I . Compare the differences in the text 'PARK' and the lampposts in *BUILDING* and faces in *PEOPLE* in I_v and I_l . Please zoom in to see the differences.

are then projected in a time sequential manner to create the edge-enhanced image. With current 3D-ready projectors with available refresh rate of 120Hz or higher, such a temporal multiplexing is imperceptible to the user. To generate the edge and non-edge images at interactive rates, we design algorithms that can exploit the parallelism offered by the GPUs.

To display the edge image at a higher resolution, we present a novel concept which we call *optical pixel sharing* (Section 3.2). This reduces the area of each projected pixel by a factor of $\frac{1}{c^2}$ while increasing their density by c^2 at the edges. Due to the sparsity of edges in most images, our optical pixel sharing unit can choose appropriate regions to be displayed at higher resolution that would minimize visible artifacts while maximizing the number of pixels reproduced at the higher resolution (Section 4). We present a statistical analysis to quantify the edge pixels rendered in higher resolution and validate the results using a large number of images of various categories. Subsequently, we find that a relatively simple optical unit consisting of an array of $c \times c$ lenses can implement optical pixel sharing effectively.

We demonstrate our enhanced resolution display in a prototype system and analyze the quality of the resulting images. Though theoretically c can be large, there are practical limits to the enhancement possible from our design – typically $c = 2$ or $c = 3$ resulting in 4 or 9 times higher resolution. Finally, this enhanced resolution is achieved by sacrificing the frame rate and the display brightness by a factor of 2. This is independent of the value of c and is due to the use of interleaved frames. However, our display can still be used in the standard low-resolution form without such a change in frame rate and brightness. We analyze several such issues in a detailed cost-benefit analysis in Section 6.

Main Contributions: We explore, for the first time, the concept of *variable spatial resolution display* – a display that does not provide uniform density of pixels everywhere but allocates higher densities at specific regions of interest based on the content. At a conceptual level, we seek to explore the fundamental question of content-specific spatial non-uniformity of resolution across a display.

Further, achieving *higher resolution images using lower resolution light modulator panels* is critically dependent on the ability to create smaller pixels. Smaller pixels when displayed at a higher density achieve true higher resolution, i.e. ability to represent higher frequency signals. Our work presents a system that uses computational optics designs to reduce the projected size of a pixel by a factor of $\frac{1}{c^2}$ while increasing its density by c^2 thereby enabling high resolution imagery from low resolution display modules.

Finally, we demonstrate the aforementioned concepts by building a laboratory prototype of enhanced-resolution gray scale projector that uses two LCD panels of resolution 512×384 to create the perception of a display of resolution 1024×768 (Figure 1). In order to generate content-specific edge and non-edge images at interactive rates we design parallel methodologies that can be easily implemented in GPUs for real-time performance.

2 Related Work

Our work builds upon a large body of literature in different domains and fills an important gap in multiple directions. Achieving higher resolution images using lower resolution light modulator panels, more commonly known as *display super-resolution*, has been the dream that has illuded the display community so far [Damera-Venkata and Chang 2009; Allen and Ulichney 2005; Aliaga et al. 2011; Jaynes and Ramakrishnan 2003; Majumder 2005]. This problem may seem analogous to that of generating a higher resolution image from multiple jittered lower resolution images, a well studied problem in the computer vision domain (detailed survey in [Babu and Murthy 2011]). However, a deeper analysis reveals them to be significantly different [Majumder 2005]. The information at a larger pixel captured at lower resolution can be thought of as encoding of multiplexed data from multiple smaller pixels that are captured at higher resolution. Hence, generating a higher resolution image from multiple jittered lower resolution images maps to a demultiplexing problem. Demultiplexing involves subtraction which in the context of displays, unlike in cameras, indicates negative light – a practical impossibility. Therefore, in displays, achieving higher resolution is dependent on generating smaller sized pixels – a hardware limitation that is impossible to overcome by software manip-

ulations alone. Hence, achieving true higher resolution, i.e. ability to display higher frequency signals, is not possible without changing the pixel size of the display [Majumder 2005]. Such a reduction of pixel size becomes available in a very limited manner on multi-projector planar displays due to projector key-stoning. The reduction of pixel size is much more significant when projecting on non-planar surfaces. Hence, recent work have proposed superimposing pixels from multiple projectors on planar or non-planar displays [Damera-Venkata and Chang 2009; Jaynes and Ramakrishnan 2003; Aliaga et al. 2011]. However, since the reduction is very limited, dependent entirely on relative position and orientation of projectors with respect to the surface, and cannot be controlled precisely, the amount of super-resolution does not scale well with the number of projectors. Even for non-planar surfaces, [Aliaga et al. 2011] report a super-resolution of 1.33 when using 3 to 4 projectors. On the other hand, wobulation based techniques use temporal multiplexing of multiple low-resolution frames, each shifted by a fraction of a pixel (usually half a pixel) [Allen and Ulichney 2005]. In all these aforementioned techniques, since the pixel size cannot be reduced much, they cannot display higher frequencies but can only achieve a high frequency boost filter during image reconstruction leading to lesser attenuation of the higher frequencies and hence a more pleasing appearance (Figures 8 and 9). In contrast, we can reduce the pixel size by a factor of c , typically $c = 2$ or $c = 3$, and hence can produce 4 or 9 times higher resolution at the edges.

The current industry has been on a rampant fervor to create more and more pixels. But the more fundamental question of how much resolution (pixel density) is needed at any spatial location is yet to be explored. Human perception studies have demonstrated our sensitivities to edges and insensitivity to very high or low spatial frequencies [Goldstein 2001; Valois and Valois 1990]. Consequently, edge sharpness, that depends both on the edge contrast and resolution [Dijk et al. 2003; Winkler 2001; Lin et al. 2006], has been used as a non-content-related parameter for object detection [Ran and Farvardin 1995] (content-related parameters being people, actions, facial expressions, etc). This has been exploited in many domains of image processing before. Edge preserving image denoising [C.Tomasi and Manduchi 1998; Durand and Dorsey 2002] compensates the loss of resolution during image filtering by retaining contrast near the edges. In image compression (e.g. JPEG compression) edge resolution is preserved by compressing those frequencies humans are less sensitive to more than the others. Similarly, in image upsampling [Kopf et al. 2007; Fattal 2007], edges have been upsampled more faithfully to retain the overall appearance. In rendering, analytically computed edges are used in combination with sparse sampling of the shading effects to generate high-quality images at interactive rates [Bala et al. 2003]. Finally, many works in non-photorealistic rendering, including silhouette and informative edges, and suggestive contours [Raskar and Cohen 1999; DeCarlo et al. 2004; Cole et al. 2009; Cole and Finkelstein 2010], have used the perceptual importance of the edges to achieve the required rendering effect. We supplement these by exploring the importance of edges in the context of displays by introducing the notion of *variable spatial resolution display* – a display that does not provide uniform pixel density everywhere but produces higher pixel densities at specific regions of the edges. While selecting these regions, our work exploits the sparsity of edges which supplements earlier works in compressive sensing [Wakin et al. 2006; Veeraraghavan et al. 2010; Sun and Kelly 2009].

The past decade has seen a tremendous activity in computational optics for capture devices [Levin et al. 2007; Liang et al. 2008; Raskar et al. 2006; Agrawal and Raskar 2007] that use optically coded images followed by computational decoding to capture additional information beyond just pixels (such as edges [Raskar et al. 2004], global and local illumination [Nayar et al. 2006], light fields

[Wilburn et al. 2005; Baker and Nayar 1999; Kuthirummal and Nayar 2006; Veeraraghavan et al. 2007], motion [Levin et al. 2008], and high dynamic range [Debevec and Malik 1997]). In the context of displays, computational optics has been explored in different contexts such as parallax barrier displays using stacked LCD panels [Lanman et al. 2010; Lanman et al. 2011; Wetzstein et al. 2011] and capture-cum-display devices [Hirsch et al. 2009]. We add to the domain of *computational displays* by using computational optics to impart additional capabilities to traditional displays.

3 Enhancement of Resolution

In this section, we describe our method to achieve an enhanced-resolution projector by selectively increasing the pixel density at the edges. First, we describe how to create the *edge-enhanced* image, I_v , that has higher resolution only at the edges (Section 3.1). I_v is formed by combining a high resolution ($cn \times cn$) *edge* and a low resolution ($n \times n$) *non-edge* image, I_e and I_{ne} , respectively. Thus, $I_v = I_e + I_{ne}$ (Figure 1) and I_e and I_{ne} are temporally multiplexed to achieve this. The selected edge pixels are displayed at a higher resolution using c^2 pixels whose size is c^2 times smaller than the regular pixels. More importantly, these images are created using spatial light modulator panels with only $n \times n$ pixels. To achieve this, we present the new computational optics model of *optical pixel sharing* (Section 3.2).

Subsequently, we show that a relatively simple optical design consisting of a grid of $c \times c$ lenses provides a practical implementation option for the optical pixel sharing unit and also follows a set of optimality criteria that we derive for this unit (Section 3.2.2). However, there are other designs for the optical pixel sharing unit which can be further investigated for different applications. Hence, we first present the general concept of optical pixel sharing and then follow it with the exact optical design that we used in our prototype (using a grid of lenses). Further, we propose an alternate optical design that can provide more freedom in the design but requires more engineering efforts to implement.

3.1 Edge-Guided Variable Resolution

Let us consider a target high-resolution $cn \times cn$ image I to be displayed by a projector. Let the high resolution coordinate system be $(s, t) \in \{1, \dots, cn\} \times \{1, \dots, cn\}$, where \times denotes the cartesian product of two sets. Consider I_l , an $n \times n$ image, created by low pass filtering I using a filter of size c in each direction. Let the low-resolution coordinate system be $(i, j) \in \{1, \dots, n\} \times \{1, \dots, n\}$. Also, each pixel (i, j) corresponds to c^2 higher resolution pixels given by $C_{ij} = \{c(i-1)+1, \dots, ci\} \times \{c(j-1)+1, \dots, cj\}$. Let E be the set of edge pixels in I_l such that at every pixel $e \in E$ we would like to display $c \times c$ smaller pixels. Let \bar{E} be complement of E and hence the set of non-edge pixels. The edge image I_e consists of all smaller pixels $\cup_{(i,j) \in E} C_{ij}$ and the non-edge image I_{ne} consists of the set of larger pixels \bar{E} . The sum of these two images provides us the *edge-enhanced* image $I_v = I_e + I_{ne}$ (Figure 1). I_e and I_{ne} are complementary to each other in terms of the pixels they display.

In order to find E , we consider the maximum CIELAB ΔE difference $h(i, j)$ between $I_l(i, j)$ and the corresponding c^2 pixels in C_{ij} which is a measure of the *local variance* within pixels C_{ij} in I . All pixels $(i, j) \in I_l$ such that $h(i, j) > T$ denote a significant perceptual difference between I_l and I . Hence, they are added to E . Clearly, the number of pixels in E , depends on the value of T . The value of T can be set to 1, 2 or 3 units of just noticeable difference (JND), where each unit of JND equals 2.3 units of ΔE difference. In the context of the displays, up to 3 JND difference is imperceptible to the human eye [Stupp and Brennesholtz 1999].

Table 1 provides a statistical analysis of the percentage of pixels in I_l that differ by more than a few JNDs from I for different categories

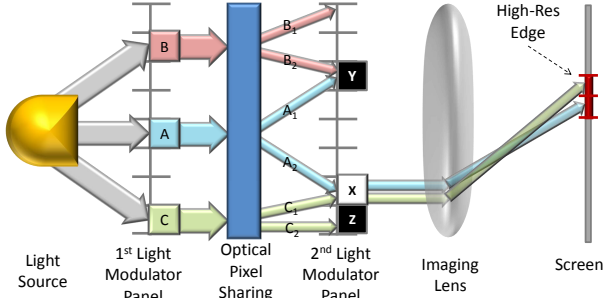


Figure 3: Displaying a perceptually high resolution image with low-resolution display modules. A , B , and C are each copied to smaller pixel pairs (A_1, A_2) , (B_1, B_2) , and (C_1, C_2) respectively. X and Y are in conflict due to A . Thus, Y is blocked (indicated by black) because X is passed (indicated by white) by the second light modulator. The simple jumbling function demonstrated here creates two copies of each pixel separated by half the size of the panel. We show in Section 3.2.2 how such a jumbling function can be implemented using a $c \times c$ grid of lenses.

of images. We observe that for $T = 3$ JND this is a small number for most images. Thus, if only a small number of pixels are displayed at higher resolution (usually less than 15%), the resulting I_v would provide a close perceptual match to I (Figure 2).

3.2 Optical Pixel Sharing

In a traditional projector, white light from the lamp illuminates a light modulator panel that spatially modulates the light to produce different pixels. A light modulator panel (either a transmissive LCD or a reflective DMD) is a regular 2D array of modulation elements or pixels, where each element can block or attenuate the light to achieve a brightness between 0 (black) and 1 (white). When assuming a linear transfer function the relationship between the input and the modulated output is linear. For single chip projectors, three channels of colors are produced by temporally multiplexing R, G and B filters placed in front of the lamp. For three-chip projectors, multiple optical paths are used for the three channels that are then combined to create the final image. We first explain our design for a grayscale digital projector, which is then extended to multiple channels in Section 3.2.3.

In order to display an edge-enhanced image, we use two cascaded and aligned low-resolution ($n \times n$) light modulator panels (e.g. LCD or DMD panels) with the optical pixel sharing unit in between them (refer to Figure 3).

Creating Smaller Pixels: The first aspect of creating higher resolution image involves creating pixels that are downsized by a factor of c in each direction. However, if n^2 pixels from the first light modulator panel are made smaller by c^2 (e.g. using a lens), there are still only n^2 pixels available at the second modulator panel filling only $\frac{1}{c^2}$ part of it. The second aspect of creating a high-resolution image thus involves creating enough smaller pixels to fill the second light modulator panel, i.e. $c^2 n^2$ smaller pixels (e.g. using c^2 lenses instead of one). Thus, every pixel will have c^2 smaller copies. However, note that if all the c^2 copies land on the same pixel of the second light modulator panel, they will not create higher resolution when passed through it. So, the key to achieve higher resolution is to have non-adjacent c^2 smaller copies of each pixel. We define the mapping between these non-adjacent copies on the second panel to the pixels they are originating from on the first panel as the jumbling function F . In our particular design, the optical pixel sharing unit is achieved by a grid of $c \times c$ appropriately designed lenses (Section 3.2.2). This implements a specific jumbling function where each pixel has c^2 smaller copies separated by $\frac{1}{c}$ distance across the panel

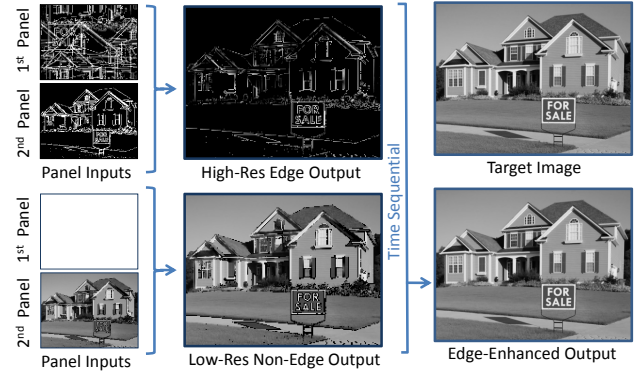


Figure 4: This figure shows the different images in the different stages of the designed system. Note that the input images are at half the resolution of the high resolution image so that they can be input to the low resolution display modules.

in each direction. This design is motivated by a set of optimality criteria discussed in Section 3.2.1. However, several other optical design can exist (Figure 10) to define different jumbling functions.

Shared Control: Since copies of c^2 pixel from the first panel fall on each pixel of the second panel, they can be only attenuated together, but not individually, using the second panel. Conceptually, each pixel in the first panel creates c^2 smaller spatially non-adjacent copies of the pixel with the same content (A controls A_1 and A_2 in Figure 3) while each pixel in the second light modulator panel attenuates c^2 spatially adjacent smaller pixels of different content (X controls A_2 and C_2). The smaller pixels from the first panel can be used to focus a high density of pixels at the desired locations on the second panel. However, there will be $c^2 - 1$ unwanted copies of each of these smaller pixels which are then blocked using the second light modulator panel. This shared control is used effectively to create the non-edge and edge image.

Creating the Non-Edge Image: Displaying the lower resolution non-edge image, I_{ne} , is relatively simple. For this, the first panel is turned ON completely and passes the light from the lamp. In this situation, the optical pixel sharing module does not have any effect and I_{ne} is used as the input to the second panel to create the non-edge pixels at lower resolution.

Creating Edge Image: In order to display the higher resolution edge image, I_e , the second panel blocks the pixels in E while passing those in \bar{E} . Hence, the input to the second panel is a low resolution binary-mask where only the pixels in E are ON.

For each edge pixel of the second panel, the first panel and the pixel sharing unit together create c^2 adjacent smaller pixels. However, these smaller pixels get their input from c^2 different pixels in the first panel. Let pixel (i, j) in the first panel be routed to the smaller pixel (s, t) in the second panel. Then the jumbling function F is defined as $F(s, t) = (i, j)$ ($F(A_2) = A$ in Figure 3). Note that F only depends on how the hardware for the optical pixel sharing is designed and not the image content. To display pixel (i', j') in the second panel at high resolution, we consider the corresponding c^2 smaller pixels in $C_{i', j'}$. For each $(s, t) \in C_{i', j'}$, we input the value of $I(s, t)$ at the location $F(s, t)$ in the first panel. Note that, due to the jumbling, adjacent pixels in the first panel can create non-adjacent pixels in the displayed image. Figure 4 illustrates the input image to the first and second panels for generating I_e and I_{ne} respectively when using a $c \times c$ grid of lenses that provide a jumbling function of $F(s, t) = (s \bmod n, t \bmod n)$.

Conflicts for Edge Image: The jumbling function F is a many-to-one function. In other words, a lower resolution pixel (i, j) in the

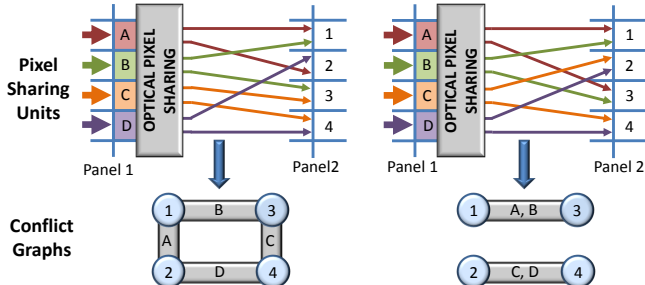


Figure 5: Two different jumbling functions and the corresponding conflict graphs. Each node denotes a low resolution pixel in the second panel. An edge between two nodes denotes a conflict. The edge is labeled with the pixel in the first panel due to which the conflict occurs. For the jumbling function on top, every pixel is in conflict with another. Hence, only one of the 4 pixels can be ON in the edge image. The jumbling function in the bottom is achieved by our optical design. This graph is a set of cliques and hence 2 of the 4 pixels can be ON in the edge image.

first modulator panel will feed many higher resolution pixels (s, t) in the displayed image. Let us assume (i, j) feeds two such higher resolution pixels: $F^{-1}(i, j) = \{(s_1, t_1), (s_2, t_2)\}$ (A feeds A_1 and A_2 in Figure 3). Since only one input can be given to the pixel (i, j) in the first panel, it can either take the value of (s_1, t_1) or (s_2, t_2) , but not both. In other words, only one of these two higher resolution pixels can be allowed to pass through the second panel to create the final image, and the other pixel has to be blocked, e.g. in Figure 3, A_2 is passed while A_1 is blocked. Let these higher resolution pixels pass through two lower resolution pixels in the second panel (i'_1, j'_1) and (i'_2, j'_2) . In other words, $(s_1, t_1) \in C_{i'_1, j'_1}$ and $(s_2, t_2) \in C_{i'_2, j'_2}$. Because of the above described scenario, only one of (i'_1, j'_1) or (i'_2, j'_2) can be kept ON. This is what we call a *conflict* (X and Y are in conflict due to A and C in Figure 3). Consequently, considering the conflicts among the pixels, only a subset of edge pixels $E_M \subset E$ can be displayed at a higher resolution. Fortunately, due to the sparsity of the edge pixels $E - E_M$ is typically a small set. Also, to assure that a pixel is not in conflict with itself, F is defined such that for any two smaller pixels $(s, t), (s', t') \in C_{i', j'}$, $F(s, t) \neq F(s', t')$.

3.2.1 Conflict Resolution

In this section, we find the maximal E_M such that there is no conflict between the pixels in E_M . This fundamentally depends on the jumbling function F and the content of I that dictates the position of the edges. We define a conflict graph, G , that has $n \times n$ vertices, each representing a pixel in the second light modulator panel. Let us consider two vertices u and v in G . Let us define the jumbling function for a set of pixels Q as $F(Q) = \bigcup_{q \in Q} F(q)$. u and v are connected if and only if $F(C_u) \cap F(C_v) \neq \emptyset$. Thus, the connectivity of G is not content-specific and depends only on F (Figure 5).

For each vertex v of G such that $v \in E$, we assign as weight, the local variance $h(v)$ (Section 3.1). For all $v \in E$, we assign weight 0. Our goal is to resolve the conflicts while retaining the visual quality as much as possible. Achieving this amounts to finding maximum independent set or the maximum weighted independent set of G .

Since G is completely dependent on the jumbling function F , we seek to design F such that it provides us with a conducive independent set for our purpose. For this, let us consider a vertex u in G . Note that the maximum cardinality of $F(C_u)$ is c^2 . Further, for each pixel $w \in F(C_u)$, there are $c^2 - 1$ other pixels v such that $w \in F(C_v)$. Thus, each pixel u in G can be in conflict with at most $c^2(c^2 - 1)$ pixels. Hence, the maximum possible degree in G is $c^2(c^2 - 1)$.

Let us now consider a G where for any two vertices u and v , either $F(C_u) \cap F(C_v) = \emptyset$ or $F(C_u) = F(C_v)$, i.e. the pixels in the

first light modulator panel from which pixel u and v in the second light modulator panel get their smaller pixels, overlap completely or none at all (Figure 5). In such a G , every pixel u will be connected to exactly $c^2 - 1$ vertices which are all connected to each other forming a clique of size c^2 . Thus, assuming n is divisible by c , G would have $\frac{n^2}{c^2}$ cliques which is also the size of its maximum independent set (assuming one pixel being chosen from each clique). Such a graph G is optimal for our purpose since (a) it minimizes the number of edges in G and hence the number of conflicts; (b) it maximizes the size of the independent set and hence the number of edge pixels that can be displayed at a higher resolution; and (c) it drastically simplifies the computation of the maximum independent set which is given by picking from each clique the vertex with the maximum h if at least one vertex of the clique belongs to E . In the following section, we demonstrate that such an optimal G and the corresponding F can be achieved using a simple optical design.

3.2.2 Optical Design

The previous section provides us the optimal connectivity or topological property for G . A desired geometric property of two conflicting pixels u and v in G is to be spatially far from each other to minimize scenarios where adjacent pixels in an edge are displayed at different resolutions. However, since this situation cannot be entirely avoided we discuss ways to alleviate the artifacts resulting from this in Section 4.2. In this section, we show that an optical design using a grid of lenses can achieve the optimal F , and thus G , respecting both the topological and geometric constraints.

Consider a $c \times c$ grid of lenses, each of focal length f . If placed at distance $d = f(1 + c)$ from the first panel, they create c^2 copies of the image of this panel focused on the second panel, each scaled by a factor of $\frac{1}{c}$ in each direction. Thus, the jumbling function is $F(s, t) = (s \bmod n, t \bmod n)$ (Figure 5) and the resulting G satisfies both the geometric and topological constraints.

The c^2 copies of the first light modulator panel should be placed contiguously without any gap or overlap. Let us assume the distance between the optical axes of two vertically adjacent lenses is r . Let us consider a pixel at vertical distances y and $r + y$ from the optical axis of the top and bottom lenses respectively. The two copies of this pixel will be at distance $\frac{y}{c}$ and $\frac{r+y}{c}$ from the optical axis of the top and bottom lenses respectively. Therefore, considering the distance r between the two axis, the distance between these two copies is given by $r + \frac{r}{c}$. Assuming a to be the height of the light modulator panels, this distance should be same as $\frac{a}{c}$. Therefore, $r = \frac{a}{1+c}$. Similarly, we can find the required horizontal distance between the optical axis of the lenses. Note that f can be chosen arbitrarily but needs to be positive to focus the image of the first light modulator panel on the second one. More information on the elements we used in practice is provided in Section 5.2.

3.2.3 Extension to Multiple Color Channels

To extend the aforementioned design to three channels, the algorithm to generate I_e and I_{ne} remains identical since we use ΔE thresholding which is valid for RGB color. However, the optical design can be extended in two different ways depending on the existing projector design architecture. For single chip architecture, our optical design can be ported as it is, by introducing a color wheel right before the first light modulator panel.

For 3-chip projector architecture [Stupp and Brennesholtz 1999], mirrors and dichroic filters are used to divide the white light into red, green and blue with three different optical paths. One panel is used for each path which are then recombined via a color bi-prism to be directed to the projection lens. The naive way to extend our design to this architecture is to use two panels with the optical pixel sharing unit in between for each of the three optical paths. This requires six panels. However, we observe that the separation be-

tween the edge and non-edge images can happen after combining the red, green, and blue images by adding the optical pixel sharing unit and a fourth panel to a traditional projector. However, to be able to project the low resolution frame, we need to bypass the optical pixel sharing unit (e.g. using moving or rotating mirrors). Since the bypassing happens at a very high frame rate, certain engineering efforts are indispensable in manufacturing such a projector.

4 Conflict Analysis

The fact that we can only display $E_M \subset E$ in high-resolution due to conflicts has consequences in terms of image quality. First we analyze the percentage of edge pixels that gets dropped due to conflict (Section 4.1). Next, even if this percentage is relatively low, the location of the dropped edge pixels ($E - E_M$) is important. If these dropped edge pixels, which are displayed at a lower resolution due to a conflict, are adjacent to a pixel in E_M which is displayed at a higher resolution, then it results in a visual artifact. We design a smoothing algorithm to alleviate such artifacts (Section 4.2).

4.1 Probability of Conflicts

Let us assume that $|E|$ constitutes a fraction f of the total pixels in I_L , i.e. $f = \frac{|E|}{n^2}$. Since the measure of local variance, h depends on c , f also depends on c . Table 1 provides the mean percentage f for a set of test images of different types for different values of c . These images were downloaded from the internet, their category assigned based on the search term used to find them. The threshold T is chosen to be between 1 and 4 JNDs. We experiment with values of c between 2 and 4 and use I_L to be of size 3072×2304 .

Let f_M denote $\frac{|E - E_M|}{|E|}$, the fraction of the total pixels that cannot be displayed at a higher resolution due to conflicts. Our goal in this section is to estimate the expected value of f_M . For simplicity, we assume the edge pixels to be distributed spatially uniformly over the image. Let us consider the conflict graph G , a set of cliques each of size c^2 , resulting from our design described in Section 3. Let us consider a vertex $v \in G$. The probability of v to be an edge pixel, i.e. $v \in E$, independent of the connectivity of G is f .

In practice, image sizes are almost always more than 1 megapixel. So, it is reasonable to assume $c^2 \ll |E|$. Now, let us consider the clique to which v belongs. The probability of having exactly k edge pixels in the $c^2 - 1$ neighbors of v in this clique is $c^{2-1}C_k f^k (1-f)^{c^2-k-1}$. Further, given that v has k neighbors, the probability of it being chosen to be displayed at higher resolution after conflict resolution, i.e. $v \in E_M$, is $\frac{k}{k+1}$. Thus, the probability of v to be displayed at high resolution when it is an edge pixel is given by

$$P(v \in E_M | v \in E) = \sum_{k=1}^{c^2-1} \frac{c^{2-1}C_k f^k (1-f)^{c^2-k-1} k}{k+1} \quad (1)$$

In order to verify this result in practice, we analyze a set of images that have different values of f and different distribution of edges. The estimated value predicted by Equation 1 matches with f_M when considering a G generated by our optical design. This is shown in Table 1. Further, to evaluate how this value changes with changes in G , we do the same experiment by considering a G where random set of pixels form the cliques instead of a structured pattern of pixels forming them as in our design. Interestingly, f_M resulting in such a G is consistently higher than that of the G provided by our optical design. We attribute this to the large spatial distance between the vertices in each clique which minimizes the possibility of having more than one $v \in E$ in the same clique.

4.2 Smoothing to Alleviate Artifacts

Due to conflicts, two adjacent edge pixels might be displayed in different resolutions. This drastic change in resolution can become perceptible, creating a visual artifact. In order to alleviate this, we

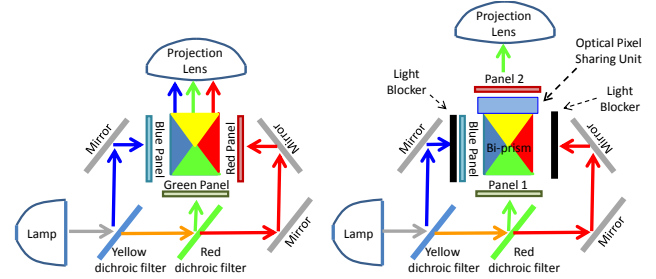


Figure 7: Design of our prototype (right) by changing a standard 3-chip projector (left). The green channel is used as the first panel. The red panel is moved between the bi-prism and the projection lens to be used as the second panel. The optical pixel sharing unit is placed between these two. The blue and red optical paths are blocked using light blockers. Note that the images generated by the prototype are green. Please check the video for illustrations.

propose a smoothing algorithm. For every pixel $(i, j) \in E$, we assign a binary weight $W(i, j)$. A weight of 1 indicates that the pixel will be displayed at high resolution and 0 indicates that the pixel will be displayed at low resolution due to a conflict i.e. $\forall (i, j) \in E_M, W(i, j) = 1$ and $\forall (i, j) \in E - E_M, W(i, j) = 0$. $\forall (i, j) \in \bar{E}, W(i, j)$ is not relevant and hence are initialized to a don't care term. The smoothing procedure smoothes the discontinuities in the relevant portions of W to create a non-binary W' , $0 \leq W'(i, j) \leq 1$ and is described in the subsequent paragraph. $W'(i, j)$ provides a weight for combining the high and low resolution content at pixel (i, j) to avoid visual artifacts. Hence, to create the final I_e , we weight the contribution from the higher resolution I_e by $W'(i, j)$ and get the rest of the contribution from $(1 - W'(i, j))I_L$. Note that for (i, j) where $W(i, j) = 0$, $W'(i, j)$ has to be kept at 0 since these pixels cannot be reproduced any better than the low resolution. Further, for pixels where $W(i, j) = 1$ the goal is to reduce the weight minimally so that high resolution content is retained maximally.

Such a smoothing cannot be achieved by a linear low pass filtering(LPF) operation since LPF both lowers hills and lifts valleys. In this case, the valleys ($W(i, j) = 0$) cannot be lifted. Interestingly, the scenario is similar to smoothing of brightness in a multi-projector display as faced in [Majumder and Stevens 2005] where the brighter pixels have to be attenuated, but the dimmest pixels cannot be brightened. Hence, we use a similar method where for each pixel (i, j) we apply $W(i, j) = \min(W(i, j), W(i+1, j) + \epsilon, W(i-1, j) + \epsilon, W(i, j+1) + \epsilon, W(i, j-1) + \epsilon, W(i+1, j-1) + \sqrt{2}\epsilon, W(i+1, j+1) + \sqrt{2}\epsilon, W(i-1, j-1) + \sqrt{2}\epsilon, W(i-1, j+1) + \sqrt{2}\epsilon)$. Multiple iterations, where all pixels perform the aforementioned operation in each iteration, provides the same result as presented by the sequential dynamic programming approach in [Majumder and Stevens 2005] to achieve an optimal W' . However, since in each iteration all pixels can be processed in parallel, this version of the algorithm can be easily implemented on the GPU (Section 5.3). The maximum number of steps required for convergence would be $\frac{1}{\epsilon}$. Typical ϵ used in our results is 0.125 which indicates 8 steps to convergence. Figure 6 illustrates W and W' and how it alleviates the visual artifacts due to conflicts.

5 Implementation and Results

We have performed two experiments to validate the feasibility of our design. We first demonstrate an enhanced-resolution projector using a 3D ready projector (Section 5.1). Next, we build a grayscale prototype by modifying an existing LCD projector (Section 5.2).

5.1 Simulation using a 3D Ready Projector

We use a BenQ MX660 3D ready single-chip DLP projector that provides 120Hz refresh rate. We consider a test image, I , at the

c	T	Architecture				People				Nature				Oil Paintings				Line Drawings			
		f	f_M^L	f_M^R	f_M^P	f	f_M^L	f_M^R	f_M^P	f	f_M^L	f_M^R	f_M^P	f	f_M^L	f_M^R	f_M^P	f	f_M^L	f_M^R	f_M^P
2	1	31	35	36	36	25	30	30	30	41	41	42	42	25	29	29	29	10	15	13	13
	2	14	17	18	18	9	11	12	12	20	23	24	24	7	9	9	9	7	12	10	10
	3	7	10	10	10	4	5	6	6	11	13	14	14	3	4	4	4	6	11	8	8
	4	4	6	6	6	2	3	3	3	6	8	9	9	1	2	2	2	5	9	7	7
3	1	56	77	78	78	54	77	77	77	66	80	80	80	59	78	78	78	15	38	36	36
	2	30	58	59	59	24	53	53	53	41	62	63	63	24	50	50	50	12	34	31	31
	3	19	44	45	45	13	35	35	35	27	49	50	50	12	29	30	30	10	31	28	28
	4	13	34	35	35	8	24	24	24	19	40	40	40	6	18	18	18	9	30	26	27
4	1	65	89	89	89	64	89	89	89	74	91	91	91	71	90	90	90	17	56	54	54
	2	40	80	80	80	35	79	79	79	51	82	82	82	36	75	75	75	14	52	50	50
	3	28	70	71	71	21	65	65	65	38	72	72	72	20	57	58	58	13	50	48	48
	4	20	62	62	62	14	52	52	52	29	63	63	63	12	42	42	42	12	49	46	46

Table 1: We collect statistics from 5 different categories of images (100 images each): Architecture, People, Nature, Oil Paintings and Line Drawings for $c = 1, 2, 3$ and $T = 1, 2, 3, 4$ JNDs. The resolution of each image is 3072×2304 . We present the mean percentage (%) of edge pixels (f), mean percentage (%) of pixels dropped due to conflicts for the lens array design (f_M^L) and a random jumbling function (f_M^R) and the predicted value of f_M^P using Equation 1 (f_M^P). Note that f_M matches closely to the predicted f_M^P and, except for the Line Drawings, the number of pixels dropped is consistently higher when using f_M^R than using f_M^L , illustrating the superior quality of the lens array design.

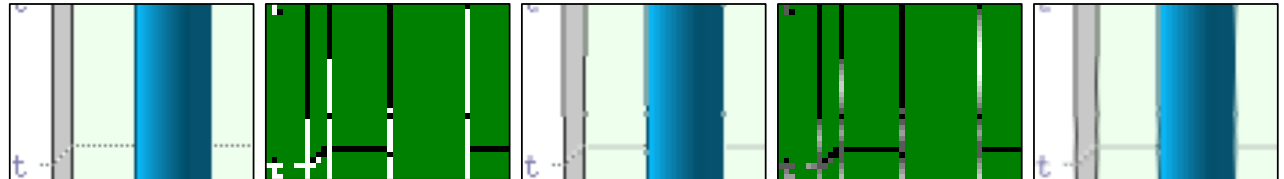


Figure 6: This illustrates the effect of our smoothing algorithm. From left to right: target high-resolution image; edge-mask before smoothing (W) contains only binary values – black denoting the pixels dropped due to conflicts, white denoting the passed pixels and green denoting the non-edge pixels that are irrelevant; edge-enhanced image before smoothing; edge mask after smoothing (W') – and the hence the gray values; and the edge enhanced image after smoothing.

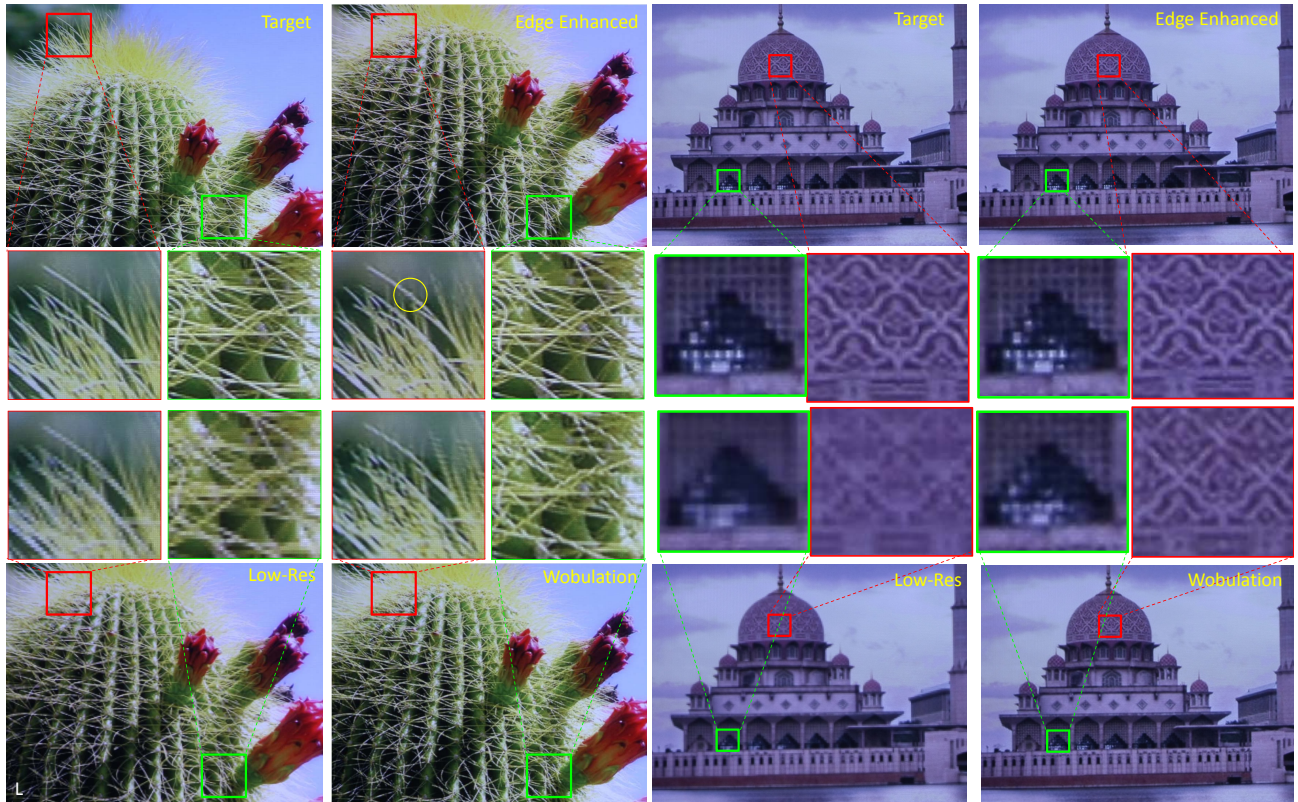


Figure 8: Two sets of images, on left and right, captured from our simulation on a 3D ready projector. From top left in a scanline order: true high resolution, edge-guided enhanced resolution, low resolution, and Wobulated image. The zoomed-in views in particular show the close match of our variable resolution image with the true high-resolution image while the low-resolution and Wobulated images fail to show the fine details. The yellow circle shows a spot where our method cannot reproduce the edge at a higher resolution due to a conflict. Please zoom in to compare different regions of the image. The images are cropped to account for the reduction from their projected size.

native resolution of the projector of 1024×768 and create the edge image, I_e , at the same resolution. We assume $c = 2$ and create the non-edge image, I_{ne} resolution 512×384 . Using this we simulate a projector with resolution 512×384 creating an enhanced resolution of 1024×768 . The non-edge image is then upscaled to the resolution of the edge image using the nearest neighbor method. These images are then projected in a time sequential manner to simulate I_v . Simulating 512×384 resolution panels allowed us to compare the result of our method with a target high-resolution image. This was also instrumental in comparing our work with wobulation [Allen and Ulichney 2005] and other similar techniques using superimposing multiple projectors [Damera-Venkata and Chang 2009; Jaynes and Ramakrishnan 2003]. Wobulation uses multiple temporally multiplexed low-resolution frames, each mechanically shifted by a fraction of a pixel (usually 0.5) to super-sample each low-resolution pixel more densely. More recently, the e-shift technology introduced by JVC achieves a fractional shift of pixels similar to wobulation using electronic means instead of mechanical ones⁴. We simulate the half pixel shift of wobulation using a shift of 1 physical pixel. We use two frames for wobulation – the usual practical choice, though 4 or 8 is possible theoretically – to avoid significant loss in frame rate and to provide a fair comparison with our method which needs to multiplex only two frames.

We capture I_v with a Canon Rebel XSi camera (4272×2848 pixels) at $\frac{1}{30}$ second exposure and I , I_e and I_{ne} at $\frac{1}{60}$ exposure. The difference in the exposure compensates for the varying brightness of these images in our design. We also capture the wobulated image for comparison. As discussed in Section 2, we demonstrate that wobulation cannot display higher frequencies (Figure 8). In contrast, our technique can produce true higher resolution (via smaller pixels) to create the closest match to a target higher resolution image (More results in the supplemental video and powerpoint slides).

5.2 Our Prototype

We also modified an Epson EMP-74 3-chip LCD projector of resolution 1024×768 to create a prototype grayscale enhanced-resolution projector for $c = 2$ (Figure 7). For this, we use the LCD panel for green channel as our first light modulator panel. Then we remove the projector lens and move the panel for the red channel outside the projector in front of the green panel to create our second light modulator panel. This panel is then connected to the input of the red panel of the projector using a ribbon cable. The blue and red light paths are then blocked and the imaging lens is placed after the second panel. This provides us with the two cascaded light modulator panels. We control the image of the first and second LCD panels by using the green and red channels of the projector respectively assuring that the two images are synchronized. An optical pixel sharing unit based on our lens array design is then placed in between the two panels. Finally, we place the projector lens in front of the second LCD panel. The labeled prototype is shown in Figure 1 and illustrated with animation in the supplementary video.

For the optical pixel sharing unit, we had to slightly modify our design since we were limited by the availability of COTS components. First, we needed a 2×2 lens array to make $c^2 = 4$ copies while commodity arrays usually provide larger grids. Therefore, we blocked all the lenslets except for a 2×2 grid in the middle. This considerably lowered the light efficiency of our prototype. Second, commodity lens arrays are not available in all different focal lengths and sizes. We used a lens array¹ with focal length of $f_1 = 41.9\text{mm}$ and lenslet size $7\text{mm} \times 5.4\text{mm}$ that was the closest to what we need. Therefore, the position of the lenslet array is guided by the requirement that the multiple copies of the image of the first LCD panel

(of size $14\text{mm} \times 10.5\text{mm}$) formed by this array should not have any gap between them. In this position, the lenslet array provides a magnification factor of 1.2 instead of the desired 0.5. Therefore, we had to use an extra lens between the lens array and the second LCD panel to scale down the pixel size appropriately. This is done using an aspheric lens with focal length of $f_2 = 30\text{mm}^2$. Then the second LCD panel is placed where the output from this lens is focused. This is achieved when the lenslet array is placed 76.8mm in front of the first LCD panel, the aspheric lens is placed 50.2mm in front of the lenslet array, the second LCD panel is placed 17.5mm in front of the aspheric lens, and finally the projection lens is placed 27mm in front of the second LCD panel. The commodity lens array (less than \$100) is designed to create a uniform illumination and not for imaging purposes. Therefore, it does not provide a uniform focus across the entire image. In order to alleviate the effect of the spatially varying defocus in our experiments, we grouped every 2×2 pixels of the projector in both of the LCD panels to provide larger pixels to alleviate the focusing issues. Thus, our projector had two panels with effective resolution of 512×384 and we created an enhanced-resolution projector of 1024×768 using these. Note that the prototype generates a green image which is converted to grayscale to generate the results in Figure 9.

In order to make sure all the elements are in focus, we use precision metric stages³ that allow us to move the elements with micron level accuracy. Due to some small radial distortion from the inexpensive lens array and rotational and translational misalignments between the panels, each pixel in the second panel could not be perfectly aligned with four smaller pixels coming from the optical pixel sharing unit. Therefore, we used standard camera-based registration procedures used in planar multi-projector displays [Chen et al. 2002; Bhasker et al. 2007] to achieve the alignment by warping the input images appropriately. Note that this registration procedure is due to the limitations common to any inexpensive lab setup. The radial distortion can be virtually removed using pairs of aspheric lenses that provide a nearly aberration free system [Stupp and Brennesholtz 1999]. Precision alignment, already standard in any 3-chip projector during combination of light from the three channels, can also be used for aligning pixels between the first and second panels.

Similar to our experiments with the 3D-ready projector, we can simulate the results of a true high resolution projector and wobulation. For this, we allow the first modulator panel to pass all the white light and input appropriate images to the second panel. Since the lens array precedes the second modulator panel, we do not face any focusing issues while projecting these images (More results in the supplemental video and powerpoint slides).

5.3 GPU Implementation

Our method to generate I_e and I_{ne} can be parallelized for efficient GPU implementation. Evaluating h at every pixel can be done in parallel. In order to compute the jumbled image, all the cliques in the conflict graph G can be processed in parallel. These generate the inputs for the two light modulator panels for I_e . To compute I_{ne} , we first low-pass-filter the image and then turn OFF the pixels belonging to E . Both these computations can be run in parallel in the GPU. The smoothing method can also be implemented in the GPU as explained in Section 4.2. We used such a GPU implementation on nVidia GeForce GTX 560 Ti to generate I_e and I_{ne} at 120fps.

6 Discussion

In this section we discuss several analysis and cost-benefit issues related to our design.

⁴<http://www.engadget.com/2011/09/08/jvc-shows-off-projectors-with-4k-precision-but-not-quite-4k-pix/>

¹<http://www.edmundoptics.com/products/displayproduct.cfm?productid=3092>

²<http://www.edmundoptics.com/products/displayproduct.cfm?productid=2953>

³<http://www.edmundoptics.com/products/displayproduct.cfm?productid=1577>

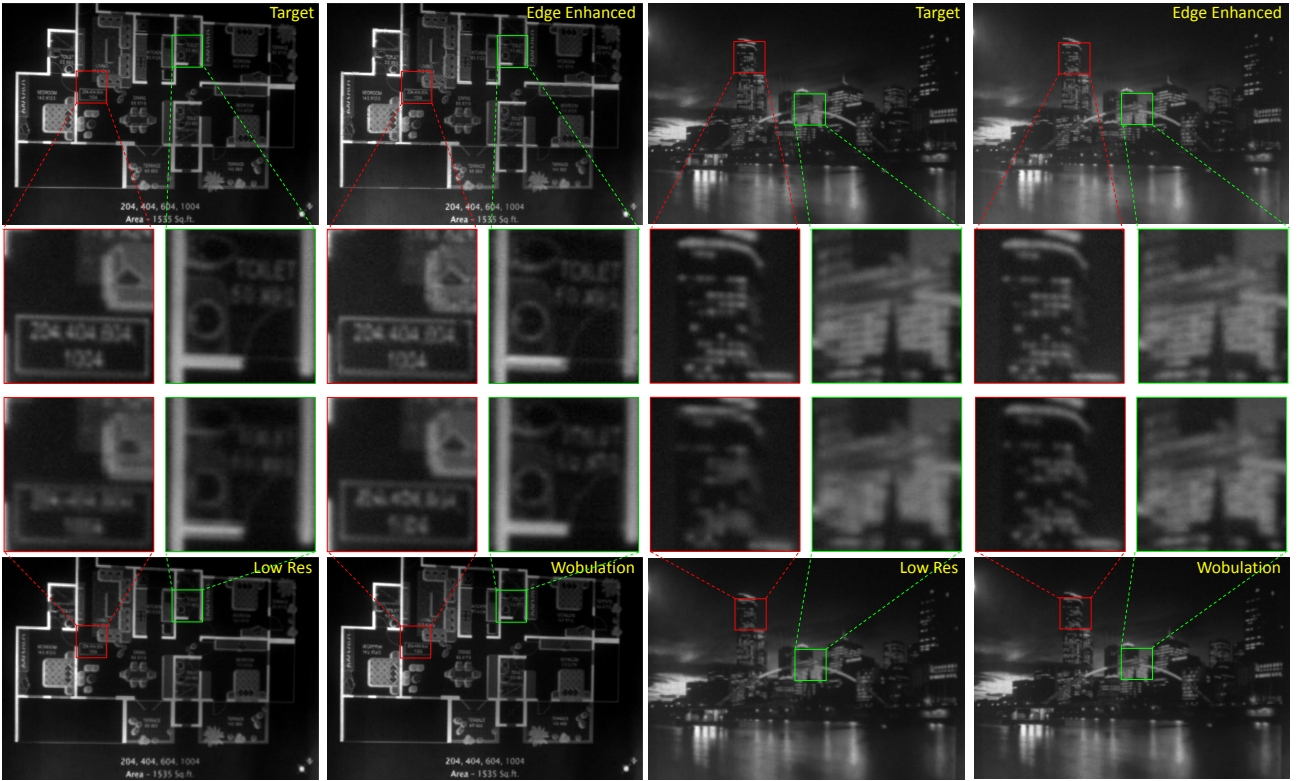


Figure 9: Two sets of grayscale images on left and right captured from our optical prototype from comparison. From left to right: true high-resolution; edge-guided enhanced resolution; low-resolution; Wobulation technique. The zoomed-in views in particular show the close match of our variable resolution image with the true high-resolution image while the low-resolution image and the Wobulation technique fail to show the fine details of the image. The images are cropped to account for the reduction from their actual projected size.

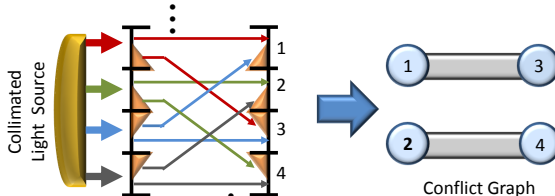


Figure 10: The picture shows the optical pixel sharing unit using the prism array design. Half of each pixel is covered by a prism. On the right we show the conflict graph for this jumbling function.

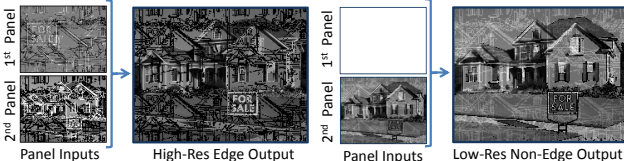


Figure 11: Modified input to the first and second light modulator panel and the resulting different I_e and I_{ne} to reduce flicker.

Alternative Optical Design: Unlike our optical design (Section 3.2.2) that provides a specific jumbling function F , here we present an alternative optical design to implement a general F . Assuming a collimated uniform light source, we use two prism arrays, one after the first light modulator panel and another before the second one. These arrays have a grid of $c \times c$ small prisms covering each pixel, each with a different angular orientation. The former prism array splits the pixels by applying different angular changes to the incoming rays. The latter provides an inverse angular change making all the light rays parallel again (Figure 10). To implement a general F , the prisms should be custom cut. Figure 10 shows a simple yet different jumbling function using this design. With this jumbling

function, pixels (s,t) , $(s+2,t)$, $(s,t+2)$ and $(s+2,t+2)$ will be copies of the same pixel in the first light modulator panel. Though the conflict graph G is topologically similar to the one achieved by our optical design (creating cliques), the locations of the copies are different. In our lens array based design, pixels (s,t) , $(s+\frac{n}{c},t)$, $(s,t+\frac{n}{c})$ and $(s+\frac{n}{c},t+\frac{n}{c})$ will be copies of each other.

However, this design is harder and more expensive to implement for two reasons. (a) It is very difficult (and expensive) to create a perfectly collimated broadband light source while collimated narrowband light sources (e.g. LED light sources used in pico-projectors) usually come at the cost of low light efficiency; and (b) it is hard to custom manufacture all the small prisms and therefore, the prisms should follow a regular pattern, as showed in Figure 10.

Extending to Video: In a projector of temporal frequency 120 fps, our method produces an acceptable video rate of 60 fps. Our first prototype using a 3D ready projector (Section 5.1) however, showed a barely perceptible flicker when viewed from close quarters. This is due to a temporal discontinuity caused by the significant difference in the global brightness of the alternating edge and non-edge images. To alleviate this, we used the pixels in the edge image which are not used to project any edges. Note that very few of the pixels (often even less than 10%) in the second light modulator panel are ON for the edge image. Since every pixel passed by the second light modulator panel results in three blocked pixels, even after considering three more conflicting pixels for each of these, more than 60% of pixels are not used. At these pixels, we divide the low resolution image between the edge and non-edge images (Figure 11). This increases the global brightness of the edge image while reducing the same for the non-edge image. Hence, the discontinuity in brightness is reduced thus removing the flicker.



Figure 12: This is the result of our method when enhancing resolution with $c = 3$ providing 9 times more pixels. For this we have to use a higher $T = 4$ JND to assure a relatively sparse edge image. This results in slight blurriness in the center of the flower. Further, since conflicts are greater in this scenario, we have marked a few of them with red. However, though our method could not reproduce all the desired edges at high resolution, the quality of the edge enhanced image is still far superior to the low-resolution image. Please zoom in to compare.

Further, the locations of the conflicting pixels (pixels in $E - E_M$) can be temporally incoherent creating visual artifacts. Hence, an extension of our smoothing algorithm (Section 4.2) to three dimensions (two spatial and one time) is needed. Our smoothing algorithm is based on the brightness smoothing algorithm presented in [Majumder and Stevens 2005] for multi-projector displays, a variant of which has been used for contrast enhancement of images and video [Majumder and Irani 2007]. We plan to explore the possibility of adapting this technique for our purpose in the future.

Image Quality Issues: In our enhanced-resolution projector, the edge image displayed at 0.5 duty cycle, is sparse and hence reduced in brightness. This leads to an overall reduction in brightness of the image. Since the black offset due to the images do not change, this reduction in the overall brightness results in a small reduction of contrast in the display. For current projectors with contrast as high as 50,000 : 1, this is a small price to pay for the increased resolution.

Limits on Enhancement of Resolution: c is a measure of the resolution enhancement achieved. Though theoretically any c is possible, the practical value of c depends on the content and the threshold T (Table 1). For almost all types of images, we find f and f_M^L to be reasonably small for $c = 2$ and $T = 3$ JND assuring a close perceptual match between a target high resolution image and our edge-enhanced image. For $c = 3$, we need to raise the threshold to be $T = 4$ JND or higher to get an acceptable value for f and f_M^L . We observe that T higher than 3 JNDs can also provide an adequate perceptual match to the target high resolution image (Figure 12). Finally, f and f_M are too high for $c = 4$ indicating that an enhancement of more than $c = 2$ or $c = 3$ is impractical.

Light Efficiency: Our design would incur some light loss due to the use of two modulators. This is a minor issue for DMDs which are very light efficient. For LCD panels too, light efficiency has improved considerably and more efforts are in progress [Lazarev and Palto 2009]. Our prototype was designed using LCD based projectors purely due to lesser difficulty in opening them up in a non-production laboratory setting. Further, the loss of light due to the alternation between the edge and non-edge frames can be alleviated by assigning unequal time slots to these two frames at the cost of a small contrast reduction for the very high contrast edges (as in [Majumder et al. 2010] for color balancing).

Diffraction: A variable resolution projector using a lens array, reduces the effective aperture size by a factor of c . However, since depth of focus is not as critical in projection as in photography most projectors use lenses with relatively high f-numbers (F/2 is typical in projection lenses). Further, most lenses, especially in high-resolution projectors (e.g. 8K Sony and Projection Design Cineo 35 projectors) are relatively large, resulting in a large effective aperture. Thus, the resolution limit from diffraction is often considerably higher than the projector resolution. However, this can become a limiting factor of our design with the increasing resolution and decreasing size in projectors. In particular, it can limit the

use of our technique to increase the resolution of pico projectors.

7 Conclusion

In conclusion, we have presented the first projector that can use $n \times n$ resolution light modulator panels to enhance the resolution at selected regions providing a perceptually close match to a target high resolution image of $cn \times cn$ where c is a small integer greater than 1. This is made possible by the novel concept of optical pixel sharing that allows selected regions of the image at the edges to be reproduced using smaller pixels with size scaled by $\frac{1}{c^2}$ at a density scaled by c^2 . Thus, we explore, for the first time, the concept of a display where pixel density changes spatially based on the content. Our prototype provides a convincing proof of concept and shows the superior perceived resolution when compared to images from standard projector with same-sized light modulator panels.

Achieving higher than HD resolution in commodity projectors today is limited by the density of pixels that can be packed in small light modulator panels. Hence, larger panels used for 4K or 8K projectors justify their cost. Though our projector allows super HD resolution in commodity projectors today, the technique is also scalable to higher resolutions of 4K and 8K projectors. More interestingly, this work opens up the concept of “resolution at demand” where resolution can be targeted at “important pixels”, like faces or humans or boundaries of foreground and background. The possibilities are numerous and can even be application specific. Thus, our work can trigger new directions for application-specific resolution retargeting in projection based displays.

Acknowledgements

We would like to acknowledge our funding source NSF CAREER IIS-0846144. We also thank our co-student at the Interactive Graphics and Visualization (iGravi) laboratory at UC, Irvine, Duy-Quoc Lai, for helping with the GPU implementation.

References

- AGRAWAL, A., AND RASKAR, R. 2007. Resolving objects at higher resolution using a single motion blurred image. *IEEE CVPR*.
- ALIAGA, D., YEUNG, Y. H., LAW, A. J., SAJADI, B., AND MAJUMDER, A. 2011. Fast high-resolution appearance editing using superimposed projections. *ACM TOG*.
- ALLEN, W., AND ULLICHNEY, R. 2005. Wobulation: Doubling the addressed resolution of projection displays. *SID*.
- BABU, R. S., AND MURTHY, K. E. S. 2011. A survey on the methods of super-resolution image reconstruction. *IJCV* 15, 2.
- BAKER, S., AND NAYAR, S. K. 1999. A theory of single-viewpoint catadioptric image formation. *IJCV* 35, 2.

- BALA, K., WALTER, B., AND GREENBERG, D. P. 2003. Combining edges and points for interactive high-quality rendering. *ACM Transactions of Graphics (Siggraph)*.
- BHASKER, E., JUANG, R., AND MAJUMDER, A. 2007. Registration techniques for using imperfect and partially calibrated devices in planar multi-projector displays. *IEEE TVCG* 13, 6.
- CHEN, H., SUKTHANKAR, R., WALLACE, G., AND LI, K. 2002. Scalable alignment of large-format multi-projector displays using camera homography trees. *IEEE Vis.*
- COLE, F., AND FINKELSTEIN, A. 2010. Two fast methods for high-quality line visibility. *IEEE TVCG* 16, 5.
- COLE, F., SANIK, K., DECARLO, D., FINKELSTEIN, A., FUNKHOUSER, T., RUSINKIEWICZ, S., AND SINGH, M. 2009. How well do line drawings depict shape? *ACM TOG* 28, 3.
- C.TOMASI, AND MANDUCHI, R. 1998. Bilateral filtering for gray and color images. *ICCV*.
- DAMERA-VENKATA, N., AND CHANG, N. L. 2009. Display supersampling. *ACM TOG* 28, 1.
- DEBEVEC, P. E., AND MALIK, J. 1997. Recovering high dynamic range radiance maps from photographs. *ACM Siggraph*.
- DECARLO, D., FINKELSTEIN, A., AND RUSINKIEWICZ, S. 2004. Interactive rendering of suggestive contours with temporal coherence. *NPAR*.
- DIJK, J., VAN GRINKEL, M., VAN ASSELT, R. J., VAN VLIET, L., AND VERBEEK, P. W. 2003. A new sharpness measure based on gaussian lines and edges. *CAIP*.
- DURAND, F., AND DORSEY, J. 2002. Fast bilateral filtering for the display of high-dynamic-range images. *ACM TOG* 21, 3.
- FATTAL, R. 2007. Image upsampling via imposed edges statistics. *ACM TOG* 26, 3.
- GOLDSTEIN, E. B. 2001. *Sensation and Perception*. Wadsworth Publishing Company.
- HIRSCH, M., LANMAN, D., HOLTZMAN, H., AND RASKAR, R. 2009. BiDi screen: A thin, depth-sensing LCD for 3D interaction using lights fields. *ACM TOG* 28, 5.
- JAYNES, C., AND RAMAKRISHNAN, D. 2003. Super-resolution composition in multi-projector displays. *PROCAMS*.
- KOPF, J., COHEN, M. F., LISCHINSKI, D., AND UYTENDAELE, M. 2007. Joint bilateral upsampling. *ACM TOG*.
- KUTHIRUMMAL, S., AND NAYAR, S. K. 2006. Multiview radial catadioptric imaging for scene capture. *ACM TOG*.
- LANMAN, D., HIRSCH, M., KIM, Y., AND RASKAR, R. 2010. Content-adaptive parallax barriers: optimizing dual-layer 3d displays using low-rank light field factorization. *ACM TOG*.
- LANMAN, D., WETZSTEIN, G., HIRSCH, M., HEIDRICH, W., AND RASKAR, R. 2011. Polarization fields: Dynamic light field display using multi-layer LCDs. *ACM TOG* 30, 6.
- LAZAREV, A., AND PALTO, S. 2009. Materials for light efficient LCD. *Society for Information Display (SID)*.
- LEVIN, A., FERGUS, R., DURAND, F., AND FREEMAN, B. 2007. Image and depth from a conventional camera with a coded aperture. *ACM TOG* 26, 3.
- LEVIN, A., SAND, P., CHO, T. S., DURAND, F., AND FREEMAN, W. T. 2008. Motion-invariant photography. *ACM TOG* 27, 3.
- LIANG, C., LIN, T. H., WONG, B. Y., LIU, C., AND CHEN, H. H. 2008. Programmable aperture photography:multiplexed light field acquisition. *ACM TOG* 27, 3.
- LIN, W. S., GAI, Y. L., AND KASSIM, A. A. 2006. Perceptual impact of edge sharpness in images. *IEEE Proceedings on Vision, Image and Signal Processing*.
- MAJUMDER, A., AND IRANI, S. 2007. Perception based contrast enhancement of images. *ACM Transactions on Applied Perception* 4, 3.
- MAJUMDER, A., AND STEVENS, R. 2005. Perceptual photometric seamlessness in tiled projection-based displays. *ACM TOG* 24.
- MAJUMDER, A., BROWN, R., AND GHOROURY, H. E. 2010. Display gamut reshaping for color emulation and balancing. *IEEE CVPR Workshop on Projector Camera Systems (PROCAMS)*.
- MAJUMDER, A. 2005. Is spatial super-resolution possible with multiple overlapping projectors? *ICASSP*.
- NAYAR, S. K., KRISHNAN, G., GROSSBERG, M. D., AND RASKAR, R. 2006. Fast separation of direct and global components of a scene using high frequency illumination. *ACM TOG* 25.
- RAN, X., AND FARVARDIN, N. 1995. A perceptually motivated three component image model: Part i. *IEEE TIP* 4, 4.
- RASKAR, R., AND COHEN, M. F. 1999. Image precision silhouette edges. *ACM I3D*.
- RASKAR, R., H TAN, K., FERIS, R., YU, J., AND TURK, M. 2004. Non-photorealistic camera: Depth edge detection and stylized rendering using multi-flash imaging. *ACM TOG* 23, 3.
- RASKAR, R., AGRAWAL, A., AND TUMBLIN, J. 2006. Coded exposure photography: Motion deblurring using fluttered shutter. *ACM TOG* 25, 3.
- STUPP, E. H., AND BRENNESHOLTZ, M. S. 1999. *Projection Displays*. Wiley.
- SUN, T., AND KELLY, K. 2009. Compressive sensing hyperspectral imager. *Computational Optical Sensing and Imaging, Optical Society of America*.
- VALOIS, R. L. D., AND VALOIS, K. K. D. 1990. *Spatial Vision*. Oxford University Press.
- VEERARAGHAVAN, A., RASKAR, R., AGRAWAL, A., MOHAN, A., AND TUMBLIN, J. 2007. Dappled photography: Mask enhanced cameras for heterodyned light fields and coded aperture refocusing. *ACM TOG* 26, 3.
- VEERARAGHAVAN, A., REDDY, D., AND RASKAR, R. 2010. Coded strobing photography: Compressive sensing of high-speed periodic events. *IEEE PAMI*.
- WAKIN, M., LASKA, J., DUARTE, M., BARON, D., SARVOHAM, S., TAKHAR, D., KELLY, K., AND BARANIUK, R. 2006. An architecture for compressive imaging. *ICIP*.
- WETZSTEIN, G., LANMAN, D., HEIDRICH, W., AND RASKAR, R. 2011. Layered 3D: Tomographic image synthesis for attenuation-based light field and high dynamic range displays. *ACM TOG* 30, 4.
- WILBURN, B., JOSHI, N., VAISH, V., TALVALA, E. V., ANTUNEZ, E., BARTH, A., ADAMS, A., HOROWITZ, M., AND LEVOY, M. 2005. High performance imaging using large camera arrays. *ACM TOG* 24, 3.

WINKLER, S. 2001. Visual fidelity and perceived quality: towards comprehensive metrics. *Proceedings of SPIE* 4299.